PHYSICAL REVIEW B **91**, 235423 (2015)

Hybrid waves localized at hyperbolic metasurfaces

O. Y. Yermakov,[*] A. I. Ovcharenko,[*] M. Song, A. A. Bogdanov,[†] I. V. Iorsh,[‡] and Yu. S. Kivshar[§]
Department of Nanophotonics and Metamaterials, ITMO University, St. Petersburg 197101, Russia
(Received 28 February 2015; revised manuscript received 24 May 2015; published 15 June 2015)

We reveal the existence of a type of surface electromagnetic wave supported by hyperbolic metasurfaces, described by a conductivity tensor with an indefinite signature. We demonstrate that the spectrum of the hyperbolic metasurface waves consists of two branches corresponding to hybrid transverse electric–transverse magnetic waves with a polarization that varies from linear to elliptic or circular depending on the wave frequency and propagation direction. The shape of the equal-frequency contours drastically depends on the frequency and changes from the elliptical to hyperbolic—a topological transition takes place. We derive asymptotic formulas describing the losses of the surface waves for capacitive, inductive, and hyperbolic regimes of the metasurface. We analyze numerically the generation of surface waves by a point electric dipole placed in the vicinity of the metasurface with numerical simulations, and also reveal wave-front peculiarities in strong anisotropic hyperbolic and σ-near-zero regimes of the metasurface.

DOI: 10.1103/PhysRevB.91.235423 PACS number(s): 42.25.Bs, 74.25.nn, 42.25.Lc, 47.55.dr

I. INTRODUCTION

Metasurfaces are known as a two-dimensional analog of metamaterials, and they offer unprecedented control over light propagation, reflection, and refraction [1,2]. One of the main advantages of metasurfaces is that these structures are fully compatible with modern planar fabrication technology and they can be readily integrated into on-chip optical devices, preserving most of the functionalities of three-dimensional metamaterials. In a general case, a metasurface can be described as a two-dimensional current characterized by a dispersive nonlocal two-dimensional conductivity tensor. At the same time, electromagnetic properties of a broad and constantly growing class of two-dimensional materials, such as graphene, silicene, and hexagonal boron nitride, can also be characterized by conductivity tensors. Thus, the physics of metasurfaces and optics of two-dimensional materials are tightly interconnected. Particularly, it has been shown in Ref. [3] that a graphene sheet can support transverse electric (TE) surface polaritons in the frequency region where the imaginary part of the surface conductivity becomes negative.

The negative imaginary part of the conductivity corresponds to the capacitive surface impedance. At the same time, the existence of TE surface waves at capacitive impedance surfaces has been studied previously [4].

In this paper, we study a special class of metasurfaces characterized by a local diagonal anisotropic conductivity tensor. Such metasurfaces can be regarded as a two-dimensional analog of uniaxial crystals. Specifically, when the imaginary parts of the principal components of the conductivity tensors have different signs, a strong correspondence appears between these structures and hyperbolic metamaterials [5]. Here, we focus on the dispersion and polarization properties of the localized waves supported by these metasurfaces.

It was shown that an anisotropic interface separating a hyperbolic metamaterial and vacuum can support a certain class of plasmonic modes analogous to the Dyakonov surface states [6–9]. Dyakonov surface states are localized modes which can propagate in a narrow angle range along the interface of the anisotropic crystals [10]. Despite their theoretical prediction back in the 1980's, these modes have been experimentally demonstrated only recently [11]. This is due to the fact that, for the case of an interface of a conventional anisotropic crystal, these modes can propagate only in an extremely narrow range of angles, and thus it is hard to excite them experimentally. Nevertheless, these modes attract significant scientific interest since they suggest a route for virtually lossless optical information transfer at the nanoscale, which is extremely important from the perspectives of on-chip optical data processing devices. Moreover, as was shown recently, the propagation direction of these modes can be effectively controlled by a slight modification of the dielectric permittivities of the structure [12].

Here, we show that, in sharp contrast to bulk hyperbolic metamaterials, hyperbolic metasurfaces can support two types of surface modes at a single frequency. These modes originate from the coupling of the transverse magnetic (TM) and TE polarized surface polaritons. A similar effect occurs in graphene sheets in the presence of a strong magnetic field perpendicular to the graphene layer [13] or on a metal substrate coated by a thin anisotropic dielectric film [14]. The corresponding surface waves have an elliptic polarization which is essential for the construction of on-chip optical networks [15–17].

II. MODEL

A. Conductivity tensor

There are different possible realizations of hyperbolic metasurfaces. In the microwave frequency range, hyperbolic metasurfaces can be realized with a certain type of *LC* contour [18,19]. In the infrared and optical range, the metasurfaces can be formed by an array of graphene nanoribbons [20] or by

[*]Present address: V. N. Karazin National University, Kharkiv 61022, Ukraine.
[†]Present address: Ioffe Institute, St. Petersburg 194021, Russia; Peter the Great St. Petersburg Polytechnic University, St. Petersburg 195251, Russia; bogdanov@mail.ioffe.ru
[‡]i.iorsh@phoi.ifmo.ru
[§]Present address: Nonlinear Physics Center and Center for Ultrahigh Bandwidth Devices for Optical Systems (CUDOS), Australian National University, Canberra ACT 2601, Australia.

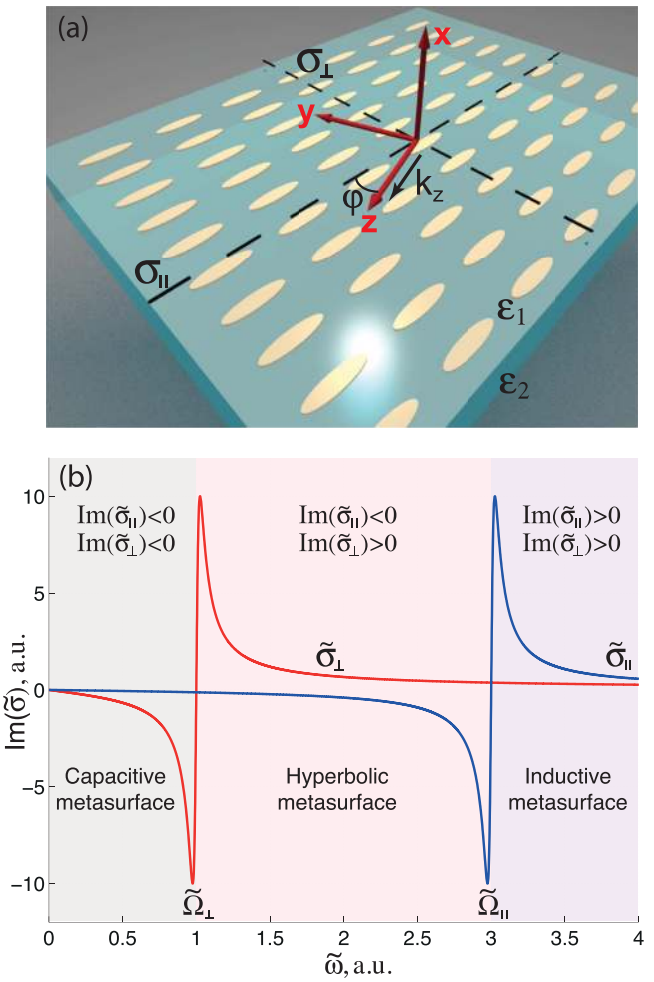

FIG. 1. (Color online) (a) Geometry of the problem. Upper ($x > 0$) half space with ε_1 and lower ($x < 0$) half space with ε_2 are separated by an anisotropic conducting layer. The principal axes of the conductivity tensor are shown by dashed lines. A surface wave propagates along the z direction. (b) Frequency dependence of the imaginary parts of dimensionless conductivity tensor components $\tilde\sigma_\perp$ and $\tilde\sigma_\parallel$. The parameters of the conductivity tensor components are $\tilde\Omega_\perp = 1$, $\tilde\Omega_\parallel = 3$, $\tilde\gamma = 0.05$.

a two-dimensional lattice of anisotropic plasmonic particles. Alternatively, metasurfaces can be formed by an array of dielectric subwavelength antennas [shown schematically in Fig. 1(a)]. This design benefits from a low level of ohmic losses in the dielectric resonators as opposed to plasmonic counterparts. At the same time, using a refractive index material such as silicon for the resonators, it is possible to achieve sufficiently subwavelength dimensions of the metasurface elements [21].

The interaction of the metasurface with an external electromagnetic field can be described with an effective conductivity tensor. Effective conductivity is directly proportional to the effective two-dimensional polarizability of the structure $\hat\alpha_{\rm eff}$ [22]:

$$\hat\sigma = (-i\omega/S_0)\hat\alpha_{\rm eff}. \tag{1}$$

Here, S_0 is a surface area of the metasurface unit cell, and ω is a frequency of the electromagnetic wave. Rigorous calculations of the effective polarizability of a two-dimensional lattice of resonant scatterers have been performed in a number of papers [23,24]. The effective polarizability of the metasurface can be expressed as

$$\hat\alpha_{\rm eff}^{-1} = \hat\alpha_0^{-1} + k_0^2\hat C(\mathbf{k},\omega). \tag{2}$$

Here, $\hat\alpha_0$ is the polarizability of the individual resonant scatterer, and $\hat C$ is the so-called dynamic interaction constant [24] which accounts for the additional polarization induced by the field scattered from all the scatterers in the lattice. In our case, a single scatterer can be approximated by a triaxial ellipsoid, for which the exact Mie series is available. However, it is justified to account only for the dipole response, which can be approximated by a Lorentzian:

$$\hat\alpha_0 = \begin{pmatrix} 0 & 0 & 0 \\ 0 & \alpha_{0,\perp} & \\ 0 & 0 & \alpha_{0,\parallel} \end{pmatrix}, \tag{3}$$

$$\alpha_{0,s} = \frac{N}{\omega^2 - \Omega_s^2 + i\gamma_s\omega}, \quad s = \parallel, \perp. \tag{4}$$

Here, N is the normalization constant, Ω_s is the resonant frequency, and γ_s is the bandwidth of the resonance, defined by ohmic and radiation losses. As can be seen in Eq. (3), we have neglected the polarizability of the scatterer in the perpendicular to the plane direction. This is justified for the sufficiently thin inclusions.

We note that by setting the right-hand side of Eq. (2) to zero we obtain the equation for dispersion of the eigenmodes of the structure $\omega(\mathbf{k})$ which accounts for both the nonlocality and finiteness of the unit cell. The rigorous analysis of the eigenmodes of the two-dimensional lattice of anisotropic scatterers is the subject of future work. Here, we would only note that, as it has been shown in Ref. [24] for a regular lattice, the radiative decay of the metasurface is allowed only in the directions satisfying the Floquet conditions $|\mathbf{k}\times\hat z|D = \pi n$, where n is an integer. Thus, for a metasurface with a period smaller than the wavelength, the losses of the surface waves are defined only by the ohmic losses in the scatterers and radiative losses caused by irregularities in the lattice geometry or by the finiteness of the sample.

Accounting only for the local response of the metasurface, and using Eqs. (2)–(4), we can write down the expressions for the effective conductivity tensor components:

$$\sigma_s(\omega) = A\frac{ic}{4\pi}\frac{\omega}{\omega^2 - \Omega_s^2 + i\gamma_s\omega}, \quad s = \perp, \parallel. \tag{5}$$

We note that such a dispersion is quite natural to many systems in the optical, infrared, THz, and radio-frequency ranges [25]. In what follows, we assume that the bandwidth of the resonant is the same for both orientations $\gamma_\parallel = \gamma_\perp = \gamma$. Constant A has a dimension of rad/s. The explicit expression of A is defined by the metasurface design. This constant can be excluded from the analysis with the help of the following dimensionless variables:

$$\tilde\sigma_s = \frac{4\pi\sigma_s}{c}, \quad \tilde\omega = \frac{\omega}{A}, \quad \tilde\gamma = \frac{\gamma}{A}, \quad \tilde\kappa = \frac{c\kappa}{A\sqrt{\varepsilon}}, \quad \tilde k_z = \frac{ck_z}{A\sqrt{\varepsilon}}. \tag{6}$$

The real part of $\tilde{\sigma}_\perp$ and $\tilde{\sigma}_\parallel$ is responsible for energy dissipation and the imaginary part is responsible for the polarizability of the structure. A typical frequency dependence of $\mathrm{Im}(\tilde{\sigma}_\perp)$ and $\mathrm{Im}(\tilde{\sigma}_\parallel)$ is shown in Fig. 1(b). One can see that the signature of conductivity tensor (7) depends on the frequency. It is possible to distinguish three cases: (i) a capacitive metasurface when both $\mathrm{Im}(\tilde{\sigma}_\perp)$ and $\mathrm{Im}(\tilde{\sigma}_\parallel)$ are negative; (ii) a hyperbolic metasurface when $\mathrm{Im}(\tilde{\sigma}_\perp)\mathrm{Im}(\tilde{\sigma}_\parallel) < 0$; and (iii) an inductive metasurface when both $\mathrm{Im}(\tilde{\sigma}_\perp)$ and $\mathrm{Im}(\tilde{\sigma}_\parallel)$ are positive which corresponds to a conventional metal sheet. It is known that both inductive and capacitive metasurfaces support the surface waves of TM and TE polarization, respectively. Thus, at $\tilde{\omega} \gg \tilde{\Omega}_\parallel$ and $\tilde{\omega} \ll \tilde{\Omega}_\perp$, the structure supports conventional TM and TE plasmons [3], respectively. However, in the intermediate region $\tilde{\Omega}_\perp < \tilde{\omega} < \tilde{\Omega}_\parallel$, the structure supports mixed TE-TM, Dyakonov-like states.

B. Dispersion equation

We consider two isotropic media with permittivities ε_1 and ε_2 separated by a hyperbolic metasurface—an anisotropic nonchiral metasurface possesses a hyperbolic dispersion at some frequency range [Fig. 1(a)]. The subwavelength size of both the resonators and the period of the structure allow one to describe the optical properties of the metasurface by a conductivity tensor, which can be represented within the local homogenization procedure as follows:

$$\hat{\sigma}_0 = \begin{pmatrix} \sigma_\perp & 0 \\ 0 & \sigma_\parallel \end{pmatrix}. \tag{7}$$

Here, $\sigma_\perp$ and $\sigma_\parallel$ are frequency-dependent conductivities per unit length corresponding to the principal axes of the tensor. We suppose that the frequency dependence of $\sigma_\perp$ and $\sigma_\parallel$ is described by Eq. (5).

We will seek a solution for the Maxwell's equations in the form of a traveling wave propagating in the z direction and localized in the x direction. Both the electric and magnetic fields depend on the z coordinate and time t as $\exp(ik_z z - i\omega t)$. We assume that φ is the angle between the z direction and one of principle axes of the tensor [see Fig. 1(a)]. The conductivity tensor is not diagonal in the chosen set of coordinates and can be written as

$$\hat{\sigma} = \begin{pmatrix} \sigma_{yy} & \sigma_{yz} \\ \sigma_{zy} & \sigma_{zz} \end{pmatrix}, \tag{8}$$

where

$$\sigma_{yy} = \sigma_\perp \cos^2\varphi + \sigma_\parallel \sin^2\varphi, \tag{9}$$

$$\sigma_{zz} = \sigma_\perp \sin^2\varphi + \sigma_\parallel \cos^2\varphi, \tag{10}$$

$$\sigma_{yz} = \sigma_{zy} = \frac{\sigma_\parallel - \sigma_\perp}{2} \sin 2\varphi. \tag{11}$$

Electric and magnetic fields (**E** and **H**) obey the following boundary conditions on the metasurface:

$$[\mathbf{n},\mathbf{H}_2] - [\mathbf{n},\mathbf{H}_1] = \frac{4\pi}{c}\hat{\sigma}\mathbf{E}, \tag{12}$$

$$[\mathbf{n},\mathbf{E}_2] - [\mathbf{n},\mathbf{E}_1] = 0. \tag{13}$$

Index 1 (2) corresponds to the upper (lower) half space, and **n** is a unit vector normal to the interface.

The dispersion equation for the surface waves can be obtained from Maxwell's equations using boundary conditions (12) and (13) and the condition where the electromagnetic field decays away from the interface,

$$\left(\frac{c\kappa_1}{\omega} + \frac{c\kappa_2}{\omega} - \frac{4\pi i}{c}\sigma_{yy}\right) \times \left(\frac{\omega\varepsilon_1}{c\kappa_1} + \frac{\omega\varepsilon_2}{c\kappa_2} + \frac{4\pi i}{c}\sigma_{zz}\right) = \frac{16\pi^2}{c^2}\sigma_{yz}^2. \tag{14}$$

Here, $\kappa_{1,2}^2 = k_z^2 - \varepsilon_{1,2}\omega^2/c^2$ is the inverse penetration depth of the surface wave into the upper and lower medium. A similar equation describes the dispersion of magnetoplasmons, surface waves in a two-dimensional electron gas in the presence of a strong dc magnetic field [13,26,27].

III. RESULTS AND DISCUSSION

A. Dispersion of surface waves

In order to analyze the dispersion of surface waves, which is described by Eq. (14), let us neglect the dissipation of the energy in the system and put $\tilde{\gamma} = 0$. The case $\gamma \neq 0$ is analyzed in Sec. III B. For the sake of simplicity, further on we will consider the symmetric situation when $\varepsilon_{1,2} = \varepsilon = 1$, but all asymptotic formulas for the dispersion and losses we will give for arbitrary ε. As an example, let us consider a structure with resonance frequencies of the conductivity tensor components $\tilde{\Omega}_\perp = 1$ and $\tilde{\Omega}_\parallel = 3$. The dependence of wave vector k_z on frequency ω and propagation direction φ can be obtained analytically from Eq. (14). This equation yields two solutions which correspond to hybrid polarized waves (quasi-TE and quasi-TM plasmons). Their dispersion for $\varphi = 60^\circ$ is shown in Fig. 2.

The surface waves of pure TE or TM polarization can propagate only along the principle axes of the conductivity

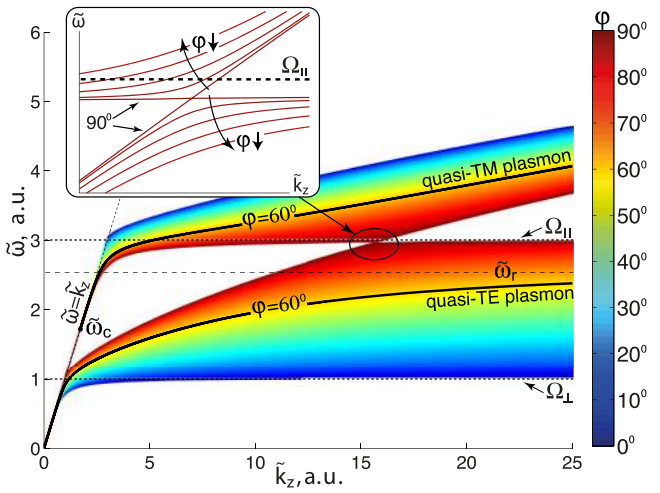

FIG. 2. (Color online) Dependence of $\tilde{k}_z$ on $\tilde{\omega}$ for the surface waves on a hyperbolic metasurface for different propagation directions φ. The two branches correspond to quasi-TM and quasi-TE surface plasmons. The inset shows the structure of dispersion curves at $\varphi \approx 90^\circ$.

tensor ($\varphi = 0^\circ$ and 90°). In this case, the right part of Eq. (14) is equal to zero and the equation splits into two independent equations corresponding to two-dimensional TE and TM plasmons [28].

The frequency cutoff of the quasi-TE plasmon is equal to zero and does not depend on φ. The frequency cutoff ω_c of the quasi-TM plasmon belongs to the interval $\Omega_\perp \leqslant \omega_c \leqslant \Omega_\parallel$ and depends on φ. This dependence can be found from the equation

$$\cot^2\varphi = -\frac{\sigma_\parallel(\omega_c)}{\sigma_\perp(\omega_c)}. \tag{15}$$

The quasi-TE plasmon has a maximal frequency ω_r at which it can propagate. The dependence of ω_r on the φ is described by the equation

$$\tan^2\varphi = -\frac{\sigma_\parallel(\omega_r)}{\sigma_\perp(\omega_r)}. \tag{16}$$

It follows from Eqs. (15) and (16) that simultaneous propagation of both surface waves at the same frequency is possible only if

$$\frac{\pi}{4} \leqslant |\varphi| \leqslant \frac{3\pi}{4}. \tag{17}$$

This condition does not depend on the specific dispersion of $\tilde\sigma_{\perp,\parallel}$ and can be fulfilled for any hyperbolic metasurface [29].

Dispersion curves of quasi-TM and quasi-TE plasmons for all angles are shown in Fig. 2. It follows from Eq. (14) and can be seen from the figure that there is a frequency gap between $\Omega_\perp$ to $\Omega_\parallel$ at an angle $\varphi = 0^\circ$. The gap is squeezed as φ tends to $\pi/2$. The structure of the dispersion curves at φ close to $\pi/2$ is shown in the inset of Fig. 2. The presence of the anticrossing means that there is a mixing of polarization. Therefore, the notation "quasi-TM" and "quasi-TE" plasmons is just formal.

The asymptotics of the dispersion for quasi-TM and quasi-TE modes can be obtained directly from Eq. (14):

$$\tilde\omega = \begin{cases} \tilde k_z & \text{for } \tilde\omega \ll \tilde\Omega_\perp \text{ (quasi-TE mode)}, \\ \dfrac{\tilde k_z^{1/2}}{(4\varepsilon)^{1/4}} & \text{for } \tilde\omega \gg \tilde\Omega_\parallel \text{ (quasi-TM mode)}. \end{cases} \tag{18}$$

These expressions coincide with the ones for two-dimensional TE and TM plasmons. In the common case, the dielectric functions of the substrate and superstate are not equal ($\varepsilon_1 \neq \varepsilon_2$). If the difference between them is small ($|\delta\varepsilon| \ll \varepsilon$), the correction to the dispersion in the symmetric case can be obtained with perturbation theory:

$$\delta k_z = \frac{\delta\varepsilon}{\varepsilon}\frac{\tilde\kappa^2}{2\tilde k_z}\left(\frac{\tilde\sigma_{yy}\tilde\omega^2 + 2i\sqrt{\varepsilon}\tilde\omega\tilde\kappa}{\tilde\sigma_{yy}\tilde\omega^2 + \tilde\sigma_{zz}\tilde\kappa^2} + \frac{\tilde\omega^2}{2\tilde\kappa^2}\right). \tag{19}$$

Figure 2 contains full information about the dispersion of the surface waves on the hyperbolic metasurface, but some peculiarities of the wave propagation associated, for example, with the density of optical states or the relative direction of the phase and group velocities, are best understood in **k** space using equal-frequency contours. Equal-frequency contours for quasi-TE and quasi-TM plasmons are shown in Fig. 3. One can see that for quasi-TE plasmons, the contours have an elliptical, ∞ shape, or a hyperbolic form depending on the frequency. Equal-frequency contours for quasi-TM plasmons

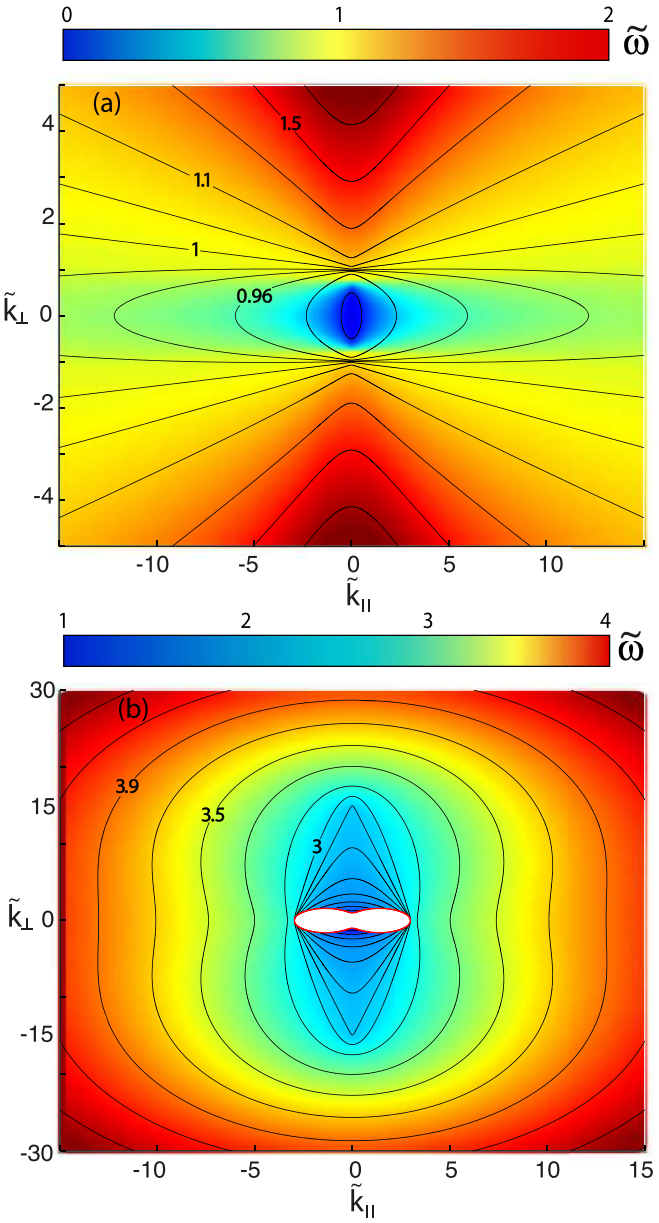

FIG. 3. (Color online) Equal-frequency contours on a **k** plane for (a) quasi-TE and (b) quasi-TM surface plasmons. Here, $\tilde k_\perp$ and $\tilde k_\parallel$ are dimensionless components of the wave vector along the principle axes of the conductivity tensor, and $\tilde\omega$ is the dimensionless frequency. In (a) $\tilde\omega$ varies from 0 to $\tilde\Omega_\parallel = 3$. In (b) $\tilde\omega$ varies from $\tilde\Omega_\perp = 1$ to infinity.

have the form of an arc, rhombus, and 8-shaped, or elliptical depending on the frequency. The arc contours are observed for the hyperbolic regime when $\tilde\Omega_\perp < \tilde\omega < \tilde\Omega_\parallel$. The end points of the arcs correspond to the frequency cutoffs $\tilde\omega_c$ which obey Eq. (15). Its solution represents a fourth-order curve in the **k** plane, a so-called *hippopede* [30]:

$$\tilde\omega_c^2 = \tilde\Omega_\perp^2 \sin(\varphi)^2 + \tilde\Omega_\parallel^2 \cos(\varphi)^2. \tag{20}$$

Discontinuity of the equal-frequency contours at the finite points which takes place for the arcs in our case is unusual for bulk waves in three-dimensional space but can be observed for

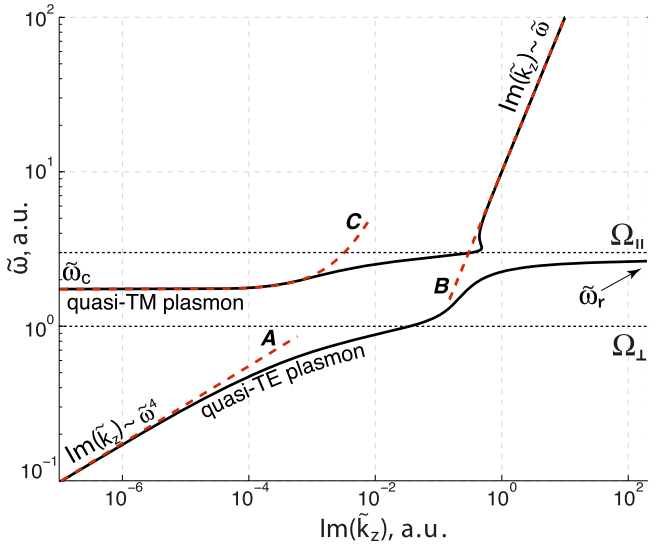

FIG. 4. (Color online) Dependence of $\mathrm{Im}(\tilde{k}_z)$ on $\tilde{\omega}$ for quasi-TE and quasi-TM surface plasmons for $\varphi = 60^\circ$ plotted on a log-log scale. Dashed lines are asymptotics of the losses described. Curve *A* is described by Eq. (21), curve *B* is described by Eq. (22), and curve *C* is described by Eq. (23).

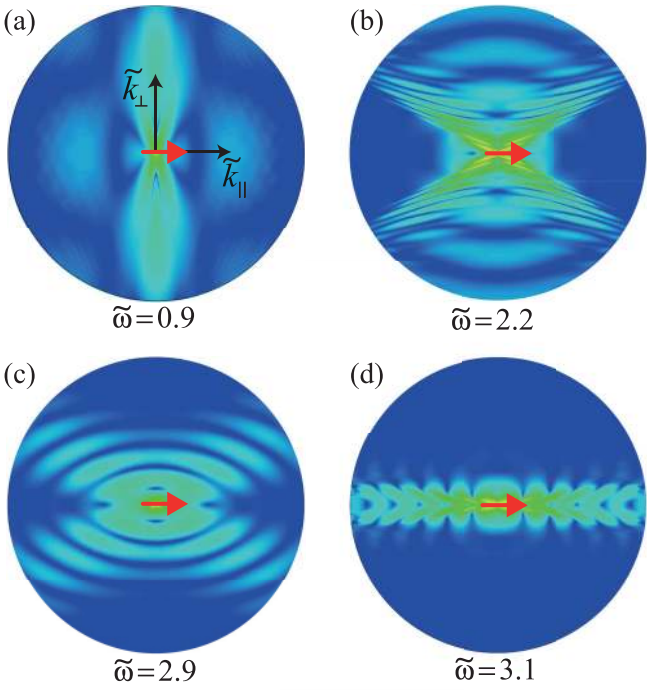

FIG. 5. (Color online) (a)–(d) Logarithmic map of the electric field amplitude for four values of normalized frequency for the case when the surface waves are excited by a pointlike electric dipole. The dipole orientation is shown with a red arrow. The metasurface conductivity spectrum is shown in Fig. 1(b).

the surface ones [10]. Points inside the hippopede correspond to the leaky quasi-TM plasmon modes.

The system considered above is similar to the one analyzed in Ref. [7] but it is two dimensional. In this sense, it is reasonable to call the waves under consideration *two-dimensional Dyakonov plasmons*.

B. Effect of losses

Let us take into account the energy dissipation and put $\tilde{\gamma} \neq 0$ in Eq. (5). It results in a finite propagation length of the surface waves which is proportional to $1/\mathrm{Im}(\tilde{k}_z)$. The frequency dependence of $\mathrm{Im}(\tilde{k}_z)$ for quasi-TE and TM plasmons is shown in Fig. 4. Using a log-log scale makes it obvious that $\mathrm{Im}(\tilde{k}_z) \sim \tilde{\omega}^4$ at $\tilde{\omega} \ll \tilde{\Omega}_\perp$ and $\mathrm{Im}(\tilde{k}_z) \sim \tilde{\omega}$ at $\tilde{\omega} \gg \tilde{\Omega}_{||}$. An asymptotic expression for $\mathrm{Im}(\tilde{k}_z)$ can be obtained from Eq. (14). In the case of $\tilde{\omega} \ll \tilde{\Omega}_\perp$, the losses can be written as

$$\mathrm{Im}(\tilde{k}_z) \approx \frac{\tilde{\gamma}\tilde{\omega}^4}{4\varepsilon}\left(\frac{\cos^2\varphi}{\tilde{\Omega}_\perp^2} + \frac{\sin^2\varphi}{\tilde{\Omega}_{||}^2}\right)\left(\frac{\cos^2\varphi}{\tilde{\Omega}_\perp^4} + \frac{\sin^2\varphi}{\tilde{\Omega}_{||}^4}\right). \quad (21)$$

In the case of $\tilde{\omega} \gg \tilde{\Omega}_{||}$, the losses can be written as

$$\mathrm{Im}(\tilde{k}_z) \approx 2\tilde{\gamma}\tilde{\omega}\varepsilon^{1/2}. \quad (22)$$

One can see that in contrast to the case of low frequencies, the losses do not depend on the propagation direction φ and resonance frequencies $\tilde{\Omega}_\perp$ and $\tilde{\Omega}_{||}$.

In the vicinity of the frequency cutoff $\tilde{\omega}_c$, the frequency dependence of $\mathrm{Im}(\tilde{k}_z)$ can be represented as

$$\mathrm{Im}(\tilde{k}_z) \approx \frac{\tilde{\gamma}\tilde{\omega}_c}{2\varepsilon^{\frac{1}{2}}} \frac{\tilde{\sigma}_{||}^2(\tilde{\omega}_c)\sin^2(\varphi) + \tilde{\sigma}_\perp^2(\tilde{\omega}_c)\cos^2(\varphi)}{1 + \tilde{\sigma}_{||}(\tilde{\omega}_c)\tilde{\sigma}_\perp(\tilde{\omega}_c)/4}\delta\tilde{\omega}. \quad (23)$$

Here, $\delta\tilde{\omega} = \tilde{\omega} - \tilde{\omega}_c$ and $\delta\tilde{\omega} \ll \tilde{\omega}_c$. One can see from Eq. (23) that $\mathrm{Im}(\tilde{k}_z) \to 0$ as $\delta\tilde{\omega} \to 0$. It is a result of weak localization of the quasi-TM plasmon near the frequency cutoff $\tilde{\omega}_c$. The opposite situation occurs for a quasi-TE plasmon mode near $\tilde{\omega}_r$ where this mode is strongly localized.

C. Field profiles

Here we perform a full-wave numerical simulation of the surface wave field profiles assuming that the surface waves are excited through the near field of a point electric dipole placed in the vicinity of the metasurface. For the simulation we use the CST Microwave Studio package. Conductivity parameters of the metasurface are taken as in Fig. 1(b). The orientation of the dipole is assumed to be along the $||$ direction [see Fig. 1(a)]. The logarithmic maps of the electric field distribution corresponding to the different excitation frequencies $\tilde{\omega}$ are shown in Figs. 5(a)–5(d).

It is well known that the shape of the wave front inherits the symmetry of the equal-frequency contour. In this sense, it is quite instructive to analyze the obtained field profiles and compare them to the equal-frequency contours shown in Fig. 3.

One can see from Fig. 3(a) that for $\tilde{\omega} = 0.9$ the equal-frequency contours are ellipses that are prolate in the $||$ direction. This is reflected in the field profile in Fig. 5(a)—the mode propagates primarily along the $\perp$ direction. This regime is analogous to the anisotropic ε-near-zero [31] regime in the three-dimensional (3D) case and can be called an anisotropic *σ-near-zero* regime.

It can be seen from Fig. 3(a) that at higher frequencies we have a topological transition, so the contours transform to hyperbolas. It results in crosslike field profiles [Fig. 5(b)]. As we have mentioned in Sec. III A, in the hyperbolic regime, both

quasi-TE and quasi-TM modes can propagate simultaneously. Indeed, in Fig. 5(b) there are two distinct wave fronts having crosslike and arclike forms that are with agreement with the equal-frequency contours shown in Fig. 3.

As we approach $\tilde{\omega} = 3$, the shape of the equal-frequency contours becomes diamondlike. In real space this corresponds to the radiation of the dipole to four distinct angles with quasiflat wave fronts [Fig. 5(c)].

Finally, at $\tilde{\omega} \gtrsim 3.0$, the equal-frequency contours have a positive curvature in the $\perp$ direction and negative in the $\parallel$ direction. It results in self-collimation of the surface wave propagating in the $\parallel$ direction. A similar effect is well known in photonic crystals [32,33]. Excitation of the surface wave in the $\perp$ direction is low-effective (in comparison with the $\parallel$ direction) because high wave vectors are needed. Therefore, the radiation of the dipole is primarily along its polarization direction [Fig. 5(d)]. Such behavior is unnatural for electric dipole radiation and is caused by the strong anisotropy of the metasurface.

D. Polarization properties

Spatial inhomogeneity and partial longitudinal polarization of surface waves results in an unusual spatial distribution of their momentum and angular momentum densities. In particular, surface waves can possess a transversal Belinfante's spin momentum [34,35]. Anisotropy of the hyperbolic metasurface results in a mixing of TE and TM surface waves and makes their polarization structure very manifold. It can be shown from the Maxwell's equations that, for the surface waves under consideration, electric field components E_z and E_y are in phase and E_x has a $\pi/2$ phase delay. It means that electric field $\mathbf{E}$ rotates in the plane orthogonal to the metasurface so that the end of $\mathbf{E}$ draws an ellipse. In the common case, the plane of the ellipse is rotated through the angle β with respect to the wave vector $\tilde{k}_z$ (Fig. 6). An equation that describes the dependence of β on $\tilde{\omega}$ and $\tilde{k}_z$ can be obtained in a closed form:

$$\tan\beta = \frac{i\tilde{\sigma}_{yz}}{2\sqrt{\varepsilon\tilde{\kappa}}/\tilde{\omega} - i\tilde{\sigma}_{yy}}. \tag{24}$$

At low frequencies ($\tilde{\omega} \ll \tilde{\Omega}_\perp$), there is only a quasi-TE mode. Therefore, angle β is close to 90° and the ellipse is almost completely degenerated into a line segment. At high frequencies, where only the quasi-TM mode propagates, angle β is near 0° and the ellipse represents a circle.

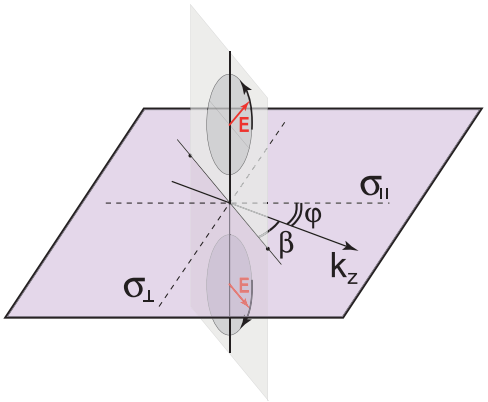

FIG. 6. (Color online) Polarization structure of hybrid surface waves on a hyperbolic metasurface.

Strong hybridization of quasi-TE and quasi-TM plasmons results in their unusual polarization. For example, for a quasi-TM plasmon at $\varphi = 11.5°$ and $\tilde{\omega} = 2.95$, angle $\beta = 87.3°$ and the difference between the semiaxis of the ellipse is less than 4%. Therefore, the wave has circular polarization. Absorption for this wave is quite low due to the vicinity of the frequency cutoff $\tilde{\omega}_c$. In this case, the figure of merit (FOM) can be estimated using Eq. (23) or numerically,

$$\mathrm{FOM} = \frac{\mathrm{Re}(\tilde{k}_z)}{\mathrm{Im}(\tilde{k}_z)} \approx 1 \times 10^5 \quad \text{for} \quad \tilde{\gamma} = 0.05. \tag{25}$$

IV. CONCLUSIONS

We have presented a comprehensive analysis of surface waves propagating along hyperbolic metasurfaces. We have analyzed the dispersion, losses, and polarization properties of such waves in the most general form, not specifying a specific design of the metasurface and describing its properties using the effective conductivity approach. Within this approach, the problem does not acquire a specific scale and, therefore, the results can be applied to different frequencies ranging from microwaves to an ultraviolet band.

We have shown that the spectrum of waves supported by hyperbolic metasurfaces consists of two branches of hybrid TE-TM polarized modes that can be classified as quasi-TE and quasi-TM plasmons. The dispersion properties of these waves are strongly anisotropic, and they have some similar features with magnetoplasmons and two-dimensional TE and TM plasmons.

Analytical solutions of the problem allow a detailed study of the surface wave properties. So, simple asymptotic formulas for the losses have been obtained near the frequency cutoff of the quasi-TM plasmon mode and in the high and low frequency regions. An analysis of the equal-frequency contours shows that their form and topology drastically depend on the frequency. The contours can have elliptic, hyperbolic, 8-shaped, rhombic, or arc form. Multiplicity of equal-frequency contours allows one to forecast in the hyperbolic metasurface such phenomena as negative refraction [36], self-collimation [33,37,38], channeling of surface waves [39,40], and large spontaneous emission enhancement of the quantum emitters due to the large density of states [41–43].

We have shown that hyperbolic metasurfaces support simultaneous propagation of both quasi-TE and quasi-TM plasmon surface modes at the same frequency, and we have derived the specific conditions for this to occur. Neither in isotropic, nor in chiral metasurfaces, is such a phenomenon known [13,27]. The polarization structure of the surface waves can vary substantially, so the polarization can change from linear to circular with different orientations of the polarization plane.

The unique electromagnetic properties of hyperbolic metasurfaces make them quite promising for applications in many areas, such as resonance sensing and detection, superlensing and near-field imaging, enhanced Raman spectroscopy, optical antennas, on-chip optical networks, etc. Taking into account their fabrication simplicity, rich functionality, and planar

geometry, it is possible to assert that hyperbolic metasurfaces can be a basis of many optical and optoelectronic devices.

ACKNOWLEDGMENTS

This work was partially supported by the Government of the Russian Federation (Grant No. 074-U01), RFBR (Project No. 15-32-20665), the Australian Research Council through Discovery and Center of Excellence Programs, and the program of Fundamental Research in Nanotechnology and Nanomaterials of the Russian Academy of Science. A.B. thanks RFBR (Project No. 14-02-01223) and the Federal Programme on Support of Leading Scientific Schools (NSh-5062.2014.2). O.Y. acknowledges support from the Dynasty Foundation. I.I. appreciates the support of the Ministry of Education and Science of the Russian Federation (Zadanie No. 3.1231.2014/K), Grant of the President of Russian Federation (MK-5220.2015.2), and Dynasty Foundation.

[1] N. Yu and F. Capasso, Nat. Mater. **13**, 139 (2014).
[2] A. V. Kildishev, A. Boltasseva, and V. M. Shalaev, Science **339**, 1232009 (2013).
[3] S. A. Mikhailov and K. Ziegler, Phys. Rev. Lett. **99**, 016803 (2007).
[4] D. Sievenpiper, L. Zhang, R. F. Broas, N. G. Alexopolous, and E. Yablonovitch, IEEE Trans. Microwave Theory Tech. **47**, 2059 (1999).
[5] A. Poddubny, I. Iorsh, P. Belov, and Y. Kivshar, Nat. Photonics **7**, 948 (2013).
[6] D. Artigas and L. Torner, Phys. Rev. Lett. **94**, 013901 (2005).
[7] Z. Jacob and E. E. Narimanov, Appl. Phys. Lett. **93**, 221109 (2008).
[8] O. Takayama, L.-C. Crasovan, S. K. r. Johansen, D. Mihalache, D. Artigas, and L. Torner, Electromagnetics **28**, 126 (2008).
[9] J. A. Polo and A. Lakhtakia, Laser Photonics Rev. **5**, 234 (2011).
[10] M. I. Dyakonov, Sov. Phys. JETP **67**, 714 (1988).
[11] O. Takayama, L. Crasovan, D. Artigas, and L. Torner, Phys. Rev. Lett. **102**, 043903 (2009).
[12] O. Takayama, D. Artigas, and L. Torner, Nat. Nanotechnol. **9**, 419 (2014).
[13] I. V. Iorsh, I. V. Shadrivov, P. A. Belov, and Y. S. Kivshar, JETP Lett. **97**, 249 (2013).
[14] I. Abdulhalim, J. Opt. A: Pure Appl. Opt. **11**, 015002 (2009).
[15] A. J. Karkar, J. E. Turner, K. Tong, A.-D. Ra'ed, T. Mak, A. Yakovlev, and F. Xia, IET Comput. Digital Tech. **7**, 294 (2013).
[16] A. Karkar, R. Al-Dujaily, A. Yakovlev, K. Tong, and T. Mak, in *Proceedings of the Fifth International Workshop on Network on Chip Architectures* (ACM, New York, 2012), p. 11.
[17] K. Ohashi, K. Nishi, T. Shimizu, M. Nakada, J. Fujikata, J. Ushida, S. Torii, K. Nose, M. Mizuno, H. Yukawa, M. Kinoshita, N. Suzuki, A. Gomyo, T. Ishi, D. Okamoto, K. Furue, T. Ueno, T. Tsuchizawa, T. Watanabe, K. Yamada, S. Itabashi, and J. Akedo, Proc. IEEE **97**, 1186 (2009).
[18] A. V. Chshelokova, P. V. Kapitanova, A. N. Poddubny, D. S. Filonov, A. P. Slobozhanyuk, Y. S. Kivshar, and P. A. Belov, J. Appl. Phys. **112**, 073116 (2012).
[19] A. V. Shchelokova, D. S. Filonov, P. V. Kapitanova, and P. A. Belov, Phys. Rev. B **90**, 115155 (2014).
[20] I. Iorsh and I. Trushkov, arXiv:1504.02130.
[21] A. I. Kuznetsov, A. E. Miroshnichenko, Y. H. Fu, J. Zhang, and B. Lukyanchuk, Sci. Rep. **2**, 492 (2012).
[22] Here and in what follows, we take the time-dependent factor as $\exp(-i\omega t)$.
[23] S. Tretyakov, A. J. Viitanen, S. I. Maslovski, and I. Saarela, IEEE Trans. Antennas Propag. **51**, 2073 (2003).
[24] P. A. Belov and C. R. Simovski, Phys. Rev. E **72**, 026615 (2005).
[25] J. D. Jackson and J. D. Jackson, *Classical Electrodynamics* (Wiley, New York, 1962), Vol. 3, p. 226.
[26] A. Ferreira, N. M. R. Peres, and A. H. Castro Neto, Phys. Rev. B **85**, 205426 (2012).
[27] K. Chiu and J. Quinn, Phys. Rev. B **9**, 4724 (1974).
[28] X. Luo, T. Qiu, W. Lu, and Z. Ni, Mater. Sci. Eng., R **74**, 351 (2013).
[29] It is necessary to mention that condition (17) is necessary but not sufficient. For the sufficiency, Eqs. (15) and (16) must be solvable for φ from Eq. (17).
[30] J. D. Lawrence, *A Catalog of Special Plane Curves* (Dover, New York, 2013), p. 143.
[31] B. Edwards, A. Alù, M. E. Young, M. Silveirinha, and N. Engheta, Phys. Rev. Lett. **100**, 033903 (2008).
[32] D. W. Prather, S. Shi, J. Murakowski, G. J. Schneider, A. Sharkawy, C. Chen, B. Miao, and R. Martin, J. Phys. D: Appl. Phys. **40**, 2635 (2007).
[33] J. Witzens, M. Loncar, and A. Scherer, IEEE J. Sel. Top. Quantum Electron. **8**, 1246 (2002).
[34] F. Belinfante, Physica **7**, 449 (1940).
[35] K. Y. Bliokh, A. Y. Bekshaev, and F. Nori, Nat. Commun. **5** (2014).
[36] C. Luo, S. G. Johnson, J. D. Joannopoulos, and J. B. Pendry, Phys. Rev. B **65**, 201104 (2002).
[37] H. Kosaka, T. Kawashima, A. Tomita, M. Notomi, T. Tamamura, T. Sato, and S. Kawakami, Appl. Phys. Lett. **74**, 1212 (1999).
[38] B. Stein, E. Devaux, C. Genet, and T. W. Ebbesen, Opt. Lett. **37**, 1916 (2012).
[39] D. Chigrin, S. Enoch, C. Sotomayor Torres, and G. Tayeb, Opt. Express **11**, 1203 (2003).
[40] P. A. Belov and C. R. Simovski, PIERS Online **1**, 37 (2005).
[41] A. N. Poddubny, P. A. Belov, P. Ginzburg, A. V. Zayats, and Y. S. Kivshar, Phys. Rev. B **86**, 035148 (2012).
[42] K. V. Sreekanth, T. Biaglow, and G. Strangi, J. Appl. Phys. **114**, 134306 (2013).
[43] K. V. Sreekanth, K. H. Krishna, A. De Luca, and G. Strangi, Sci. Rep. **4**, 6340 (2014).